Temperature-induced membrane trafficking drives antibody delivery to the brain

Fusheng Du[1], Qi Wan[1], and Oleg O. Glebov[2]*

[1] Institute of Neuroregeneration and Neurorehabilitation, Qingdao University, Qingdao 266071, Shandong, China.

[2] Department of Psychological Medicine, Institute of Psychiatry, Psychology & Neuroscience, King's College London, De Crespigny Park, London SE5 8AF, UK.

*ooglebov@gmail.com

Highlights

- Temperature increase of 2-3°C upregulates endocytosis and exocytosis
- Temperature-induced upregulation of membrane trafficking requires protein translation and dynamin function
- Mild whole-body hyperthermia enhances fluid-phase endocytosis across the body
- Mild hyperthermia enables delivery of an exogenous antibody from the bloodstream into the brain through a dynamin-dependent pathway

Abstract

Despite quotidian occurrence of fever and hyperthermia, cell biological mechanisms underlying their effects remain unclear. Neurological complications of severe (>40°C) fever have been associated with increased blood-brain barrier (BBB) permeability due to structural disruption, while little is known about brain physiology of moderate fever. Here, we show that a temperature increase to 39-40°C triggers fluid-phase uptake in PC12 cells and primary neurons. Uptake of selective cargoes shows that clathrin-mediated endocytosis and macropinocytosis are induced in a translation-dependent manner, consistent with a role for heat shock response. Exocytic recycling is also increased by hyperthermia, suggesting a comprehensive boost of membrane trafficking. Mild (<39°C) whole-body hyperthermia *in vivo* boosts fluid-phase uptake in various organs, notably enabling brain accumulation of an intravenously injected antibody that is blocked by dynamin inhibition. Taken together, our findings show that fever systemically regulates membrane trafficking across the body, reveal dynamin-dependent endocytosis as an innate cell biological mechanism for temperature control of BBB permeability, and demonstrate a clinical potential of mild hyperthermia for facilitating brain delivery of biologic drugs.

Introduction

Heat profoundly affects the functioning of the living matter through the commonly encountered phenomena of fever and hyperthermia. Fever constitutes an evolutionarily conserved response to injury and infection that is centred around controlled increase in body temperature, believed to confer protection against pathogens (1–3), and hyperthermia refers to uncontrolled increase in body temperature due to heat accumulation (4, 5). At its extreme, high fever above 40°C is considered dangerous as a medical emergency (*2*, *3*, *6–12*), while severe environmental hyperthermia represents an increasingly prevalent cause of mortality and morbidity due to the effects of global climate change (*4*, *13*, *14*). Conversely, most cases of fever and hyperthermia involve moderate temperature elevations to 39-40°C, associated with beneficial physiological and clinical outcomes (*15–17*). Despite the prominence of fever and hyperthermia in and out of the clinic (*18*, *19*), the cell biological effectors of temperature on physiology remain poorly understood.

The brain is particularly affected by fever and hypothermia, owing to its environmental sensitivity and metabolic demands. Temperatures above 40°C are associated with structural damage to the brain, in particular affecting the blood brian barrier (BBB) - a specialised layer of endothelial cells separating the bloodstream from the brain space (*3*, *7–9*, *9–11*, *20–22*). Considering that delivery of macromolecules into the brain is normally severely restricted by the BBB (*23*), thermal treatment has a potential for aiding drug brain delivery, especially relevant for large biologic drugs such as immunoglobulins that cannot efficiently cross the BBB under normal conditions (*24–26*). Implementation of this approach would however necessitate combining BBB permeabilization with tissue damage mitigation (*20*, *21*, *27–29*), warranting deeper understanding of the cell biology underlying the physiological impact of temperature on the brain.

Membrane trafficking represents a key cell biology mechanism for drug delivery across the BBB, whereby cargo is endocytosed from the bloodstream and exocytosed into the brain milieu, providing the transcellular route of delivery (*24*, *30*). While this process is normally tightly controlled, allowing only limited transport of specific cargoes, ageing promotes non-specific transcytosis of various cargoes across the BBB (*31*), highlighting the potential for intrinsic membrane trafficking to transport macromolecules without overt BBB disruption. Based on early ultrastructural evidence (*32*) and our recent findings demonstrating temperature effects on endocytosis in neurons (*33*), we hypothesised that moderate temperature regimes may regulate membrane trafficking in the brain.

Results

To investigate the general link between temperature and membrane trafficking, we investigated the effects of 3 hours treatment with hypothermia (19-23°C) and hyperthermia (39-40°C) in the rat pheochromocytoma 12 (PC12) cell line which is routinely used in neuroscience and pharmacology studies. Calcein-AM/PI staining showed that neither hypothermia nor hyperthermia significantly affected cell viability (**Figure S1A, B**). 3 hours of hyperthermia led to a robust increase in uptake of a fluid phase marker 4 kDa dextran labelled with fluorescein isothiocyanate (FITC), henceforth referred to as 4 kDa FITC-dextran, while hypothermia had no effect (**Figure 1A, B**). The effect of hyperthermia was confirmed using a structurally unrelated fluorescent fluid-phase marker dye Lucifer yellow, suggesting that the effect was not limited to dextran uptake (**Figure S1C, D**).

Immunostaining for endosomal marker proteins early endosomal antigen 1 (EEA1) and lysosome-associated marker protein 1 (LAMP1) revealed that hyperthermia downregulated early endosomes and enhanced late endosomes, while hypothermia downregulated early but not late endosomes (**Figure 1C-E**), showing that different temperatures altered the capacity of endosomal compartments. Hyperthermia but not hypothermia also increased F-actin levels (**Figure 1F, G**), consistent with the role for actin dynamics in endocytosis (*34*). Based on these observations, we sought to investigate hyperthermia-induced membrane trafficking in more detail.

To investigate the role of specific pathways involved in hyperthermia-induced endocytosis, we focused on the two key endocytic pathways in PC12 cells, namely clathrin-mediated endocytosis (CME) involved in uptake of many receptors and ligands, and macropinocytosis providing internalisation of large fluid volumes and high molecular weight cargoes (*35*). We found that hyperthermia increased uptake of FITC-labelled iron-binding protein transferrin (Tf), a specific CME cargo, and this uptake was inhibited by pharmacological blockade of a key CME regulatory protein dynamin by an antidepressant drug sertraline (*36*) (**Figure 2A,B**), confirming the upregulation of CME. Uptake of a selective macropinocytosis marker TRITC- 70 kDa dextran (*37*) was also enhanced following hyperthermia, while application of a macropinocytosis blocker 5-(n-ethyl-nisopropyl)-amiloride (EIPA) prevented this increase (**Figure 2C, D**). Hyperthermia-induced increase was observed for an even larger probe 2MDa FITC-dextran, although uptake of the latter was limited by its molecular weight (**Figure S2A, B**). Taken together, these results indicate that hyperthermia upregulates both CME and macropinocytosis in PC12 cells.

For further mechanistic understanding of hyperthermia-induced endocytosis, we evaluated the role for heat shock response, an evolutionarily conserved mechanism involving translation of heat shock proteins (*38*, *39*). Translation blocker anisomycin abolished hyperthermia-induced uptake of Tf (**Figure 2E, F**) and 70 kDa TRITC-dextran (**Figure 2G, H**). Immunostaining showed an increase in levels of the canonical heat shock proteins Hsp70 and Hsc70 that was also abolished by anisomycin treatment (**Figure S2C-F)**, confirming that 39-40°C hyperthermia was sufficient to induce the heat shock response and reaffirming the role of heat-shock response in hyperthermia-induced membrane trafficking. To investigate the effects of hyperthermia on membrane trafficking in differentiated polarised cells, we quantified uptake in primary neurons. Much like in PC12 cells, hyperthermia significantly increased endocytosis of both Tf and 70 kDa TRITC-dextran in primary neurons in a translation-dependent manner (**Figure S3A-C**). SThese data show that hyperthermia treatment increased endocytosis in polarised cell types.

To test the effects of hyperthermia on exocytosis, we pre-loaded cells with Tf and measured loss of intracellular fluorescent signal over time. After 20 minutes, the rate of fluorescence loss in cells subjected to hyperthermia was significantly increased in comparison to the control cells, indicating that exocytic recycling of endocytosed Tf was more enhanced by hyperthermia than Tf endocytosis (**Figure 3A, B**). For 70 kDa dextran, rate of fluorescence loss in hyperthermia-treated cells was not significantly different from the control cells, indicating that hypothermia-induced increase in fluid-phase endocytosis was matched to that in endocytosis (**Figure 3C, D**). Taken together, these data show that hyperthermia enhances exocytosis as well as endocytosis.

On the basis of the above evidence for hyperthermia-induced membrane trafficking in cultured cells, we sought to establish its role in transport across biological barriers *in vivo*. To this end, we induced whole-body hyperthermia (WBH) in mice (*40*) and measured penetration of distally administered markers 4 kDa dextran and Evans blue into various organs as described by us recently (*41*). The WBH protocol induced a temperature increase to 38.3-39°C within 3 hours (**Figure 4A, B**), equivalent to mild fever and well below the temperature range associated with structural damage to the tissue. We found that there was a trend towards increased accumulation of 4 kDa dextran in multiple organs including the brain (**Figure 4C, D**), although in this exploratory experimental sample of 6 animals per condition the effect only reached the threshold for statistical significance in the liver and heart (**Figure S4A, B**). While normothermic control animals showed no signs of brain permeation by Evans blue, WBH treatment induced significant Evans blue accumulation (**Figure 4C, E**), consistent with induction of BBB permeability by WBH.

To further investigate the translational relevance of WBH-induced BBB permeability, we sought to test whether it can enable uptake of larger biologically relevant macromolecules and, if so, whether this process involves membrane trafficking. The two main membrane trafficking pathways for transcellular uptake are CME and caveolae, both of which require dynamin function (*24*). We therefore investigated uptake of an immunoglobulin (Ig) and 70 kDa dextran, using dynamin block by sertraline to confirm the role for membrane trafficking. As expected, WBH robustly induced brain accumulation of Ig which was abolished by sertraline injection, indicating that Ig was was transported in a dynamin-dependent manner (**Figure 4F, G**). Conversely, WBH did not result in significant uptake of 70 kDa dextran, suggesting that macropinocytosis was not induced and that BBB integrity was unaffected (**Figure 4F, H**). Taken together, these results show that membrane trafficking induced by mild WBH requires dynamin function and can carry immunoglobulins from the bloodstream into the brain.

Discussion

Our study provides a key mechanistic insight into the cell biology of fever and hyperthermia in the brain. To thi day, physiologically relevant temperature regimes of mild fever and hyperthermia in the brain have remained understudied, the focus of investigation being on decidedly pathological extremes (*4*, *5*, *8*, *11*). Our work fills this gap in knowledge, showing that increases in temperature less than 2°C in magnitude can elicit profound changes in the pathways of membrane trafficking and suggesting a simple model explaining the effects of mild-to-moderate fever/hyperthermia on the BBB permeability (**Figure 4I**). More broadly, a common cell biological basis underlying the wide-ranging physiological impacts of febrile temperature range across the body is likely to have far-reaching implications, given the central role of membrane trafficking in health and disease (*30*).

The physiological role of membrane trafficking in fever remains to be established. Temperature-induced induction of macropinocytosis reported here is consistent with enhanced phagocytosis and activation of lymphocytes (*42*) (*43*) and may upregulate other relevant pathways, e.g. at the immunological synapse (*44*, *45*) or in fever-associated immune signalling pathways such as cytokine signalling (*46–48*). Further, membrane trafficking is likely to contribute to a wide range of fever-associated processes, including endocytosis of pathogens (*49*), processing of pathogens by relevant immune cells, cell

migration, and extravasation. More generally, upregulation of membrane trafficking may provide a compensatory mechanism to counter the deleterious effects of temperature increase across the body, e.g. by stimulating lysosomal clearance of misfolded proteins (*50*). Conversely, a sufficiently high increase in temperature may result in dysregulation of membrane trafficking, contributing to adverse effects of hyperthermia and high fever (*11*). Direct testing of these predictions will require manipulation of temperature-induced membrane trafficking, e.g. by dynamin inhibitors, in physiologically relevant experimental models of mild and severe fever.

Our data show that temperature-induced membrane trafficking is associated with expression of heat shock proteins and requires protein biosynthesis. This evidence is consistent with canonical heat shock response (*38*), rather than translation-independent processes such as hypothermia-induced synaptic enhancement (*33*) or regulation of cytosolic viscosity (*51*), yet a role for other temperature sensors *e.g.* ion channels cannot be explicitly ruled out (*52*, *53*). Mechanistically, heat shock proteins could regulate endocytosis via direct interaction between heat shock proteins and CME machinery (*54*) (*55*), actin dynamics (*56*), and directly with biomembranes (*57*, *58*), or indirectly through protein phase separation (*59–61*). For now, the molecular mechanism coupling heat shock response with membrane trafficking remains unclear, warranting further investigation.

Finally, the finding that hyperthermia induces wide-ranging enhancement of endocytosis *in vivo*, specifically in the brain the basis of our findings, it is conceivable that membrane trafficking under a low-febrile temperature regime can be co-opted into a general delivery protocol compatible with a wide variety of drugs. Considering the fever below 39°C in adults is generally regarded as safe (*1*, *11*), this alternative approach would obviate most if not all concerns associated with drug delivery across the BBB. Crucially, our evidence directly confirms the validity of this approach for brain delivery of antibodies, the currently dominant class of biologics (*62*). Although it remains to be seen whether mild fever can increase BBB permeability in humans, in due course our findings may inform development of forward clinical trials towards febrile-aided delivery of biologics into the brain, as well as other hard-to-reach tissues of the body.

Declaration of interests

None declared.

Figure titles and legends

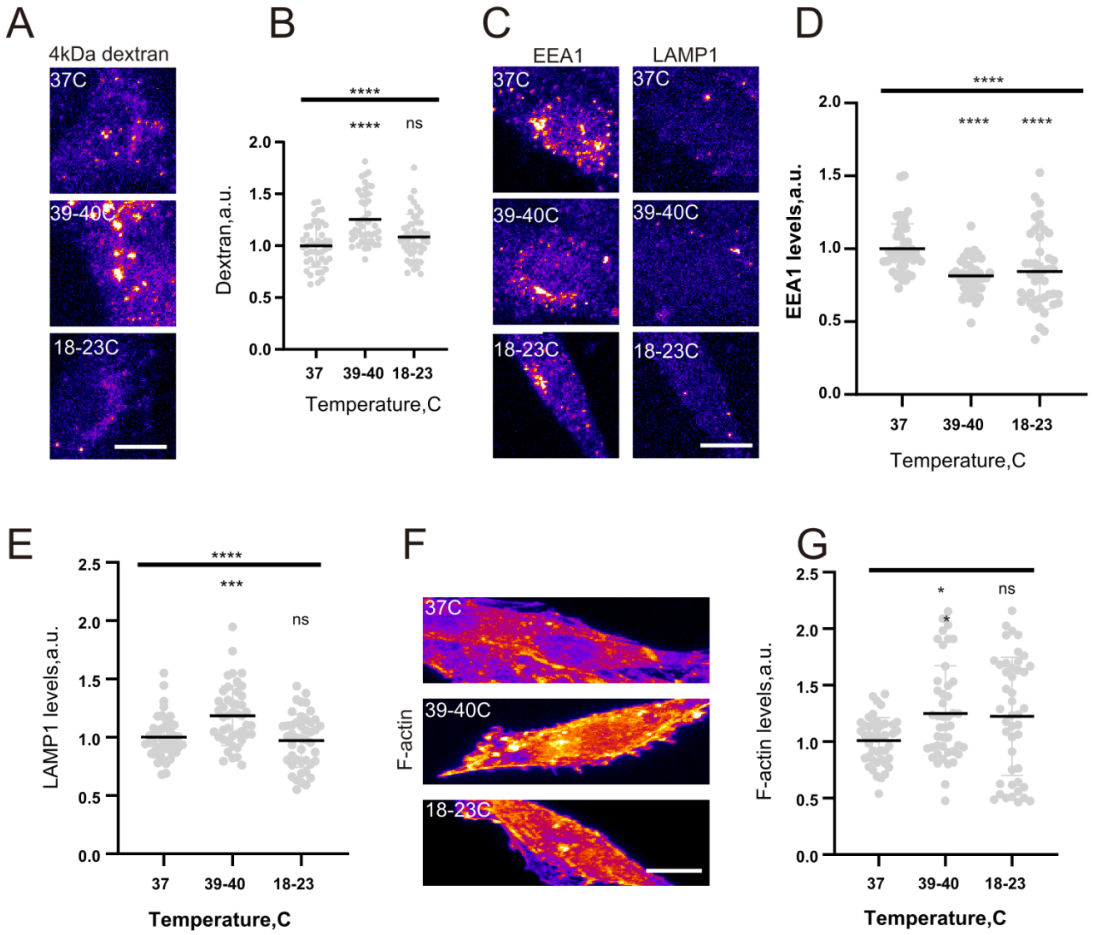

Figure 1. Different temperature regimes regulate endocytosis and endosomes

(A) Representative images of 4kDa dextran internalisation in PC12 cells treated with different temperatures for 3 hours.

(B) Quantification of 4kDa dextran internalisation in PC12 cells treated with different temperatures for 3 hours. ****P < 0.0001, ns-not significant, Kruskal–Wallis test with Dunn's multiple comparisons test.

(C) Representative images of PC12 cells treated with different temperatures for 3 hours and immunostained for EEA1 and LAMP1.

(D) Quantification of EEA1 levels in PC12 cells treated with different temperatures for 3 hours. ****P < 0.0001, Kruskal–Wallis test with Dunn's multiple comparisons test.

(E) Quantification of LAMP1 levels in PC12 cells treated with different temperatures for 3 hours. ****P < 0.0001,***P < 0.001, ns-not significant, Kruskal–Wallis test with Dunn's multiple comparisons test.

(F) Representative images of PC12 cells treated with different temperatures for 3 hours and stained for F-actin.

(G) Quantification of F-actin levels in PC12 cells treated with different temperatures for 3 hours. *P < 0.05, ns-not significant, Kruskal–Wallis test with Dunn's multiple comparisons test.

N ≥ 3 independent experiments, n ≥ 45 cells. Scale bar, 10 μm.

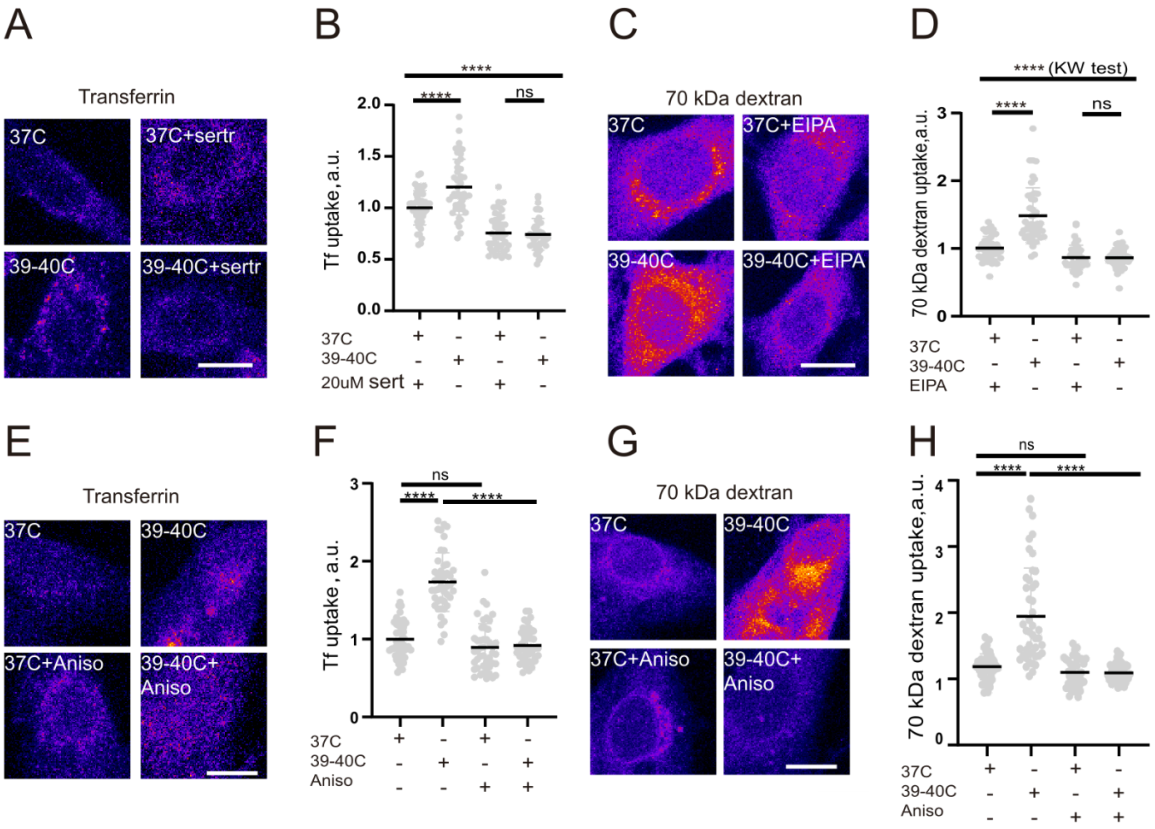

Figure 2. Hyperthermia induces CME and macropinocytosis in a translation-dependent manner

(A) Representative images of FITC-transferrin internalisation in PC12 cells with 20μM sertraline for 15 min after hyperthermia for 3 hours.

(B) Quantification of FITC-transferrin internalisation in PC12 cells with 20 μM sertraline for 15 min after hyperthermia for 3 hours. ****P < 0.0001, ns-not significant, Kruskal–Wallis test with Dunn's multiple comparisons test.

(C) Representative images of 70 kDa TRITC-dextran internalisation in PC12 cells with 25μM EIPA after hyperthermia for 3 hours.

(D) Quantification of PC12 cells incubated with 25μM EIPA after hyperthermia for 3 hours. ****P < 0.0001, ns-not significant, Kruskal–Wallis test with Dunn's multiple comparisons test.

(E) Representative images of 70kDa dextran internalisation in PC12 cells treated with hyperthermia for 3 hours and anisomycin.

(F) Quantification of 70kDa dextran internalisation in PC12 cells treated with hyperthermia for 3 hours and anisomycin. ****P < 0.0001, ns-not significant, Kruskal–Wallis test with Dunn's multiple comparisons test.

(G) Representative images of FITC-transferrin internalisation in PC12 cells treated with hyperthermia for 3 hours and anisomycin.

(H) Quantification of FITC-transferrin internalisation in PC12 cells treated with hyperthermia for 3 hours and anisomycin. ****P < 0.0001, ns-not significant, Kruskal–Wallis test with Dunn's multiple comparisons test.

N ≥ 3 independent experiments, n ≥ 45 cells. Scale bar, 10 μm.

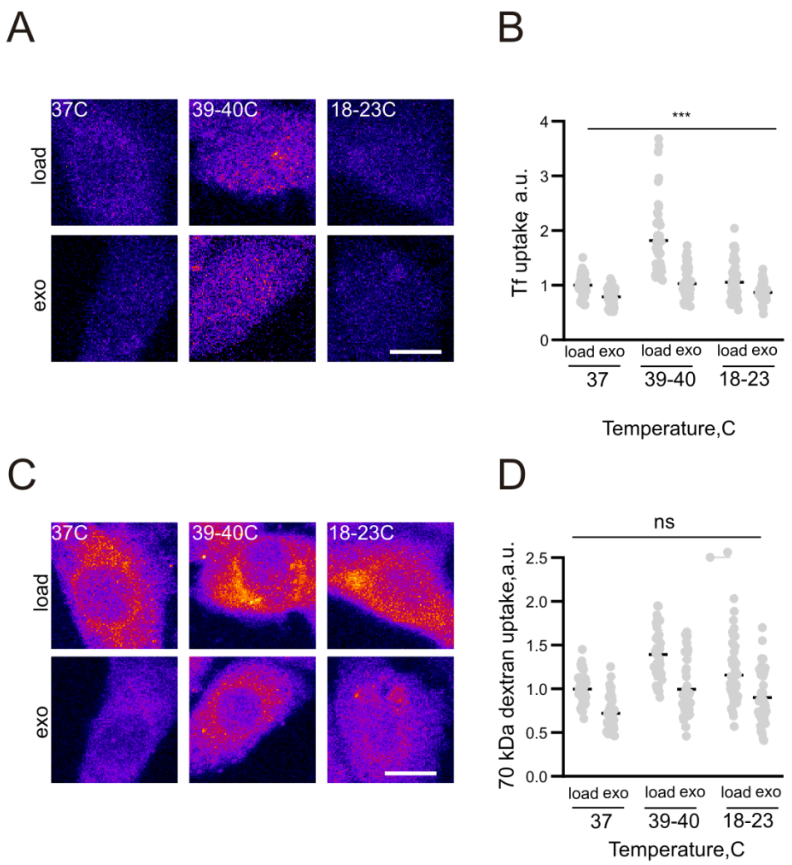

Figure 3. Hyperthermia induces exocytosis as well as endocytosis

(A) Representative images of Tf exocytosis in PC12 cells treated with different temperatures. Load - cells loaded with Tf for 1 hour, exo - cells loaded with Tf for 1 hour following 20 min in Tf-free medium.
(B) Quantification of FITC-transferrin exocytosis in PC12 cells treated with different temperatures. ***P < 0.001 for the effect of temperature, 2-way ANOVA.
(C) Representative images of 70 kDa dextran exocytosis in PC12 cells treated with different temperatures. Load - cells loaded with Tf for 1 hour, exo - cells loaded with Tf for 1 hour following 20 min in Tf-free medium.
(D) Quantification of 70 kDa TRITC-dextran exocytosis in PC12 cells treated with different temperatures. ns, no significant effect of temperature, 2-way ANOVA. N ≥ 3 independent experiments, n ≥ 45 cells. Scale bar, 10 μm.

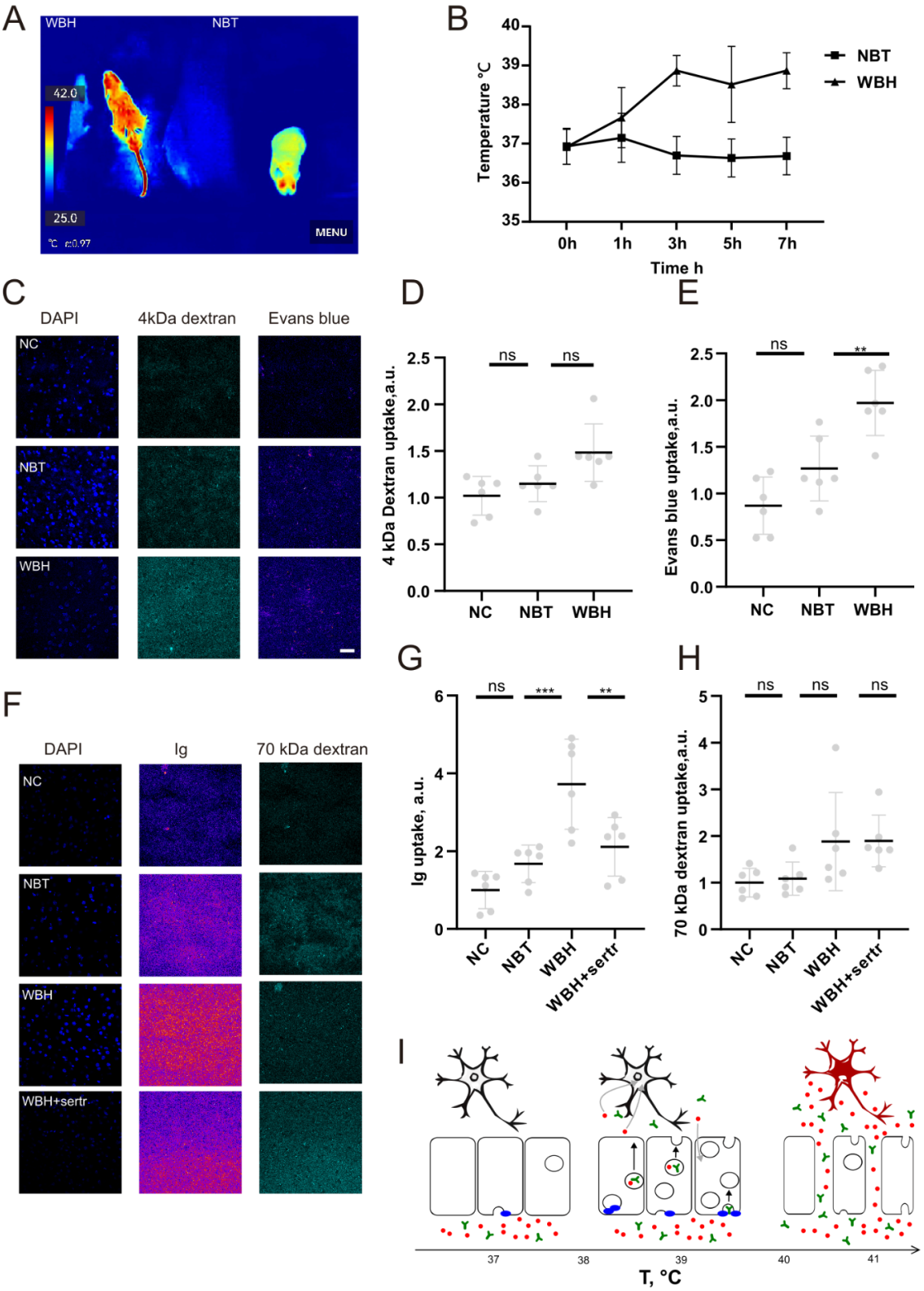
A
WBH
NBT
42.0
25.0
MENU
B
Temperature °C
40
39
38
37
36
35
0h
1h
3h
5h
7h
Time h
NBT
WBH
C
DAPI
4kDa dextran
Evans blue
NC
NBT
WBH
D
4 kDa Dextran uptake,a.u.
ns
ns
NC
NBT
WBH
E
Evans blue uptake,a.u.
ns
**
NC
NBT
WBH
F
DAPI
Ig
70 kDa dextran
NC
NBT
WBH
WBH+sertr
G
Ig uptake, a.u.
ns
***
**
NC
NBT
WBH
WBH+sertr
H
70 kDa dextran uptake,a.u.
ns
ns
ns
NC
NBT
WBH
WBH+sertr
I
37
38
39
40
41
T, °C

Figure 4. Hyperthermia induces transcytosis across the BBB in mouse brains

(A) Representative image of WBH in mice. Left, mouse subjected to whole body hyperthermia (WBH); right, control mouse with normal body temperature (NBT).
(B) Time course of WBH induction in mice.
(C) Representative image of cortical brain sections from mice with injected 4 kDa FITC-dextran and Evans blue. NC, negative control (no injection).
(D) Quantification of brain uptake of 4 kDa dextran. Ns, no significant, 1-way ANOVA with Dunn's multiple comparisons test. Data was normalised to the signal in NC.
(E) Quantification of brain uptake of Evans blue. **P<0.01, 1-way ANOVA with Dunn's multiple comparisons test. Data was normalised to the signal in NC.
(F) Representative images of cortical brain sections from mice with injected Ig and 70 kDa dextran .
(G) Quantification of brain uptake of Ig. ***P<0.001, **P<0.01, ns - not significant, 1-way ANOVA with Dunn's multiple comparisons test. Data was normalised to the signal in NC.
(H) Quantification of brain uptake of 70 Da dextran. ns - not significant, 1-way ANOVA with Dunn's multiple comparisons test. Data was normalised to the signal in NC.
(I) Schematic model representing the physiological effects of fever/hyperthermia on the BBB. Ig (immunoglobulin, green) represents macromolecules of interest for brain delivery, glutamate (red) represents undesirable molecules to be excluded from the brain. At ***normal body temperature (left)***, transcytosis through the BBB is repressed, restricting ingress of both Ig and glutamate into the brain space. Under conditions of ***mild fever/hyperthermia (middle)***, membrane trafficking requiring activity of dynamin (blue) is induced, enabling transcellular route of Ig and possibly glutamate to the brain. Due to limited capacity of transcytosis, glutamate is effectively removed from the extracellular milieu through the action of glutamate transporters, preventing excitotoxicity. In ***severe fever/hyperthermia (right)***, structural integrity of the BBB is compromised, resulting in massive uncontrolled entry of both Ig and glutamate into the brain, resulting in glutamate-induced excitotoxicity and cell death.

Tables with titles and legends

Antigen	Species	Conjugation	Manufacturer	Cat. No.	Dilution
EEA1	rabbit		Abcam	ab2900	1/300
LAMP1	mouse		Invitrogen	MA1-164	1/300
Rabbit IgG	goat	Alexa Fluor 488	Bioss	Bs-0295 G-AF488	1/500
Mouse IgG	goat	Alexa Fluor 594	SolarBio	K1031G-AF 594	1/500
HSP70	rabbit		Boster	BA0928	1/400
HSC70	mouse		Boster	M01024-1	1/400

GABAAR	rabbit		Synaptic Systems	224203	See Methods

Methods

Reagents, drugs, fluorescent markers

Cell culture materials were from Solarbio and Procell. ICR mice and Sprague-Dawley rats were from Jinan Pengyue Laboratory Animal Co. 4 kDa FITC-dextran and 2 MDa FITC-Dextran were from Sigma-Aldrich. 70 kDa TRITC-dextran was from Chondrex Inc. FITC-Transferrin was from Jackson Immunoresearch. Lucifer yellow was from Santa Cruz. Anisomycin and doxorubicin was from Macklin. EIPA was from Selleck. Evans blue was from Solarbio. Sertraline and Apoptozole was from AbMole. 647 phalloidin was from Yeasen Biotechnology. Calcein-AM/PI Double Staining Kit was from Meilun. Rabbit immunoglobulin (Ig) was from Synaptic Systems.

Cell culture

PC12 cells were grown and maintained in high glucose Dulbecco's Modified Eagle medium (DMEM) (Solarbio) containing 10% foetal bovine serum (FBS) (Procell/Gibco) and 1% penicillin/streptomycin (Gibco) at 37°C in a humidified incubator with 5% CO2. PC12 cells were seeded into 24-well culture plates (3×104 cells/well, Corning Costar) at a density of 50-60% for temperature treatment and subsequent cell uptake, immunocytochemistry and Phalloidin staining. Primary rat neuronal cultures were isolated and maintained according to the standard Banker method (*63*).

Temperature treatment and membrane trafficking assays

After the PC12 cells had grown in 24-well plates and reached 50-60% confluence, they were used for experimentation. Cells were exposed to hypothermia (18-22°C), normothermia (37°C) and hyperthermia (39-40°C) for 3 hours, using dedicated cell incubators. Culture medium was high glucose DMEM (Solarbio) containing 20 mM HEPES, used at 500 µl per well. Same treatment was applied to neurons, except the culture medium was Neurobasal (Gibco) with B27 and glutamine.

After treatment at different temperatures for 3 hours, fluorescently labelled compounds were added via a change of medium, and cells were transferred to the 37°C incubator for uptake. After uptake, cells were fixed with 4% paraformaldehyde (PFA) and washed six times with phosphate buffer (PBS) for five minutes each. Slides were then mounted in Fluoromount-G mounting medium (Southern) and stored at 4°C until imaging. Final concentrations of 4 kDa FITC-dextran, 70 kDa TRITC-dextran, 2 MDa FITC-dextran, Tf, Lucifer yellow were 1 mg/ml, 1 mg/ml, 2 mg/ml, 5 µg/ml, 1 mg/ml respectively. EIPA was used to block macropinocytosis at a concentration of 25 µM, sertraline was used to block CME at a concentration of 20 µM, and anisomycin was used at 5 µg/ml.

To measure exocytosis, cells were washed three times with 500ul of empty medium and then incubated with medium containing 70 kDa FITC-dextran or transferrin at a final concentration of 1 mg/ml. fitc-dextran for 1 hour at 37°C. Subsequently, cells were removed from the

incubator, washed three times with 500 ul culture medium, and then either fixed immediately in 4% PFA (no exocytosis control) or incubated with new culture medium for 20 min at 37°C and then fixed as above. Cells were mounted in Fluoromount-G and stored at 4°C until imaging.

Whole body hyperthermia in vivo

All mice were intraperitoneally injected with 0.1 ml saline. The whole body hyperthermia group (WBH) was put into a heating box, and the temperature was increased by 0.5°C every 15 min to 39°C and maintained at this level for 6 hours. Once per 2 hour period, all mice were placed at room temperature for a 15 min rest, while rectal temperature was measured and 0.1ml saline was injected intraperitoneally. Rectal temperature was measured at a final rest for thermal imaging. Normal body temperature (NBT) and negative control groups (NC) were maintained at room temperature (18-22°C), with the same procedures for injection and temperature measurement as described above. All animals were sacrificed one hour later. The brains were fixed with 4% PFA, cut into into 25 or 30 μm thick sections with a frozen slicer, mounted onto positively-charged microscope slides in media containing 4′,6-diamidino-2-phenylindole (Solarbio), and imaged using a confocal microscope.

Blood-brain barrier measurements in vivo

For measurement of blood-brain barrier permeability on Evans blue and 4 kDa FITC-dextran, ICR mice (8-10 weeks old, male, weighing 28-32 g) were randomly allocated into the whole body hyperthermia group (WBH), normal body temperature (NBT) and negative control groups (NC). Evans blue and 4 kDa FITC-dextran were dissolved in PBS and injected into the tail vein. The dosage of FITC-dextran was 200 μg/kg, while Evans blue was administered as a 2% solution at 4 ml/kg. Equal volumes of PBS were injected into the NC treatment at room temperature.

For measurement of blood-brain barrier permeability on immunoglobulin and 70 kDa TRITC-dextran and the effect of sertraline on its permeability. ICR mice were randomly allocated into groups as above plus the whole body hyperthermia group with sertraline (WBH+sertr). Sertraline was dissolved in PBS and injected intraperitoneally at dosage of 10 mg/kg; other groups were injected with an equal volume of PBS. 3 hours after the sertraline injection, Ig and 70 kDa TRITC-dextran were dissolved in PBS and injected into the tail vein in dosages of 20 μg/kg and 200 μg/kg respectively. Temperature treatment and other operations were as above.

Immunocytochemistry and Phalloidin staining

After temperature treatment, cells were transferred to room temperature and washed once in PBS. Coverslips were fixed with 4% PFA in PBS for 20 min and afterwards washed six times in PBS. For blocking, coverslips were incubated with 0.3% Triton-X 100 in PBS supplemented with 5% goat serum for 60 min. Following the primary antibody incubation for 2 hours, coverslips were washed six times in PBS, and incubated with Alexa Fluor 488 and Alexa Fluor 594 conjugated secondary antibodies for 1 hour. After 6 more washes in PBS, coverslips were mounted onto slides in Fluoromount-G mounting medium and stored at 4°C until imaging. The antibodies used in this study are listed in **Table S1**. For staining with

phalloidin, coverslips were fixed and blocked as described above, then incubated with 1/2000 phalloidin for 2 h, washed six times in PBS, then mounted and stored as above.

Confocal microscopy imaging

Samples were imaged on Nikon Eclipse Ti2 laser confocal microscope equipped with a standard set of lasers and objectives. The imaging systems were controlled by NIS Elements 2.0 software. The imaging parameters for Nikon Eclipse Ti2 were as follows. The following image acquisition settings were used for serial confocal z-stack images: cells - 1.5 µm step, 512 x 512 pixels, 1x zoom, 100x magnification; tissue sections - 0.5 µm step (short-term assay) or 1.5 µm (long-term assay) 512 x 512 pixels, 1x zoom, 40x magnification. Pinhole size was kept at a suitable (1-2AU) Airy unit. Excitation laser wavelengths were 488 nm ,561 nm and 647 nm. Bandpass filters were set at 500−550 nm (FITC, Alexa Fluor 488) and 570−620 nm (TRITC, AlexaFluor 594) and 650−750nm (Alexa Fluor 647). Gain, exposure and offset settings were optimised within each experiment to ensure appropriate dynamic range, low background and optimal signal/noise ratio.

Statistical analysis

Statistical analysis was carried out using the GraphPad Prism v5 (https://www.graphpad.com/). Data distributions were assessed for normality using d'Agostino and Pearson omnibus normality tests. For normally distributed datasets, two sample t test, 1-way ANOVA, with Dunn's, Bonferroni's post tests and 2-way ANOVA were used to assess statistical significance as appropriate; for non-normally distributed datasets, Mann-Whitney rank test, Kruskal-Wallis test and Dunn's post test were used. The data sets are presented in the form of scatter plots, bar plots and line plots, with plot averages as lines. All the experiments were performed in at least 3 independent experiments as detailed in figure legends.

Supplemental Figures

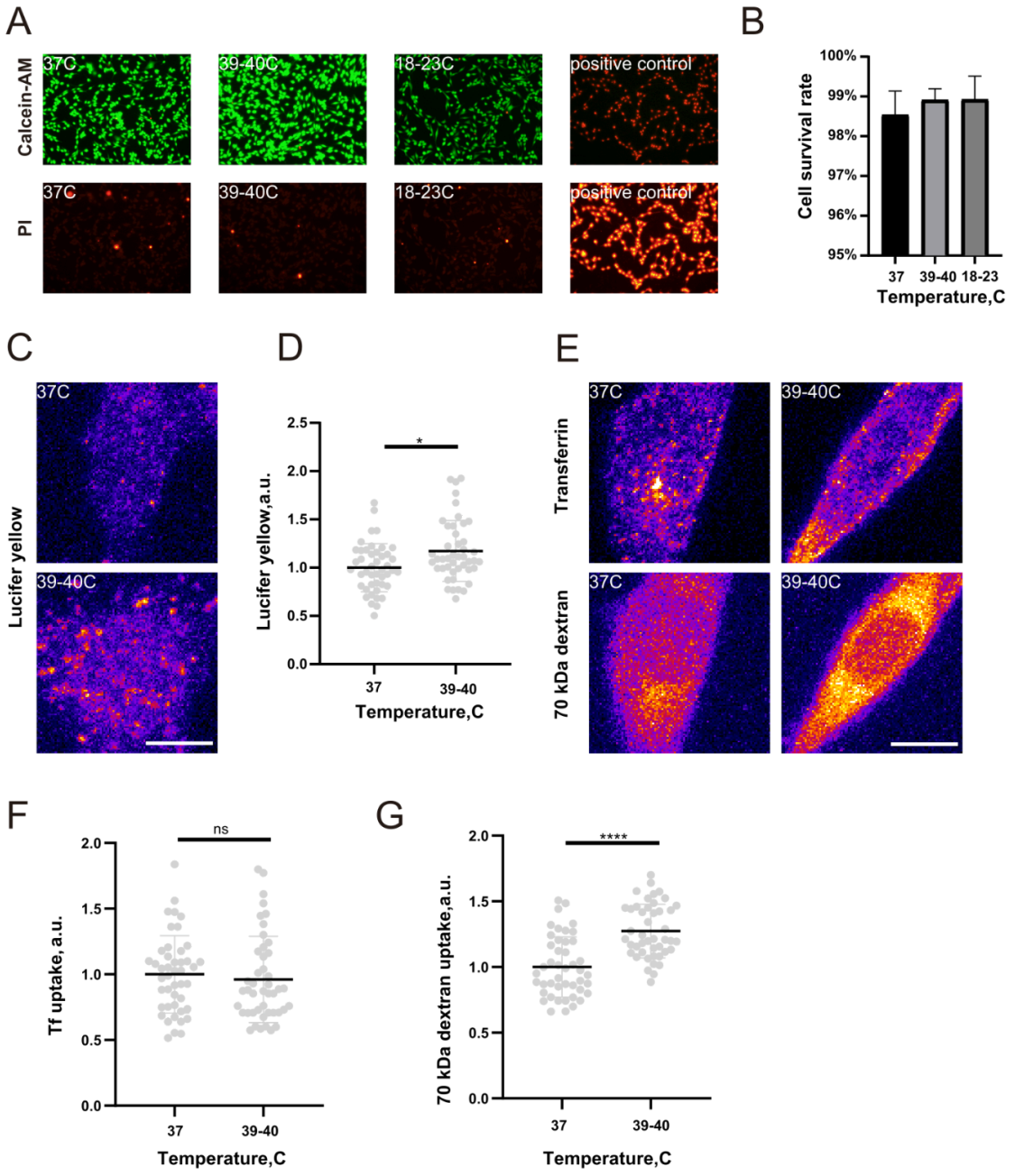

Figure S1

(A) Representative images of Calcein-AM/PI double stained in PC12 cells treated with different temperatures for 3 hours. Scale bar, 200 μm.

(B) Rate of cell survival in each image of PC12 cells treated at different temperatures for 3 hours.

(C) Representative images of Lucifer yellow internalisation in PC12 cells treated with hyperthermia for 3 hours. N ≥ 3 independent experiments, n ≥ 45 cells. Scale bar, 10 μm.

(D) Quantification of Lucifer yellow endocytosis.*P < 0.05, Mann–Whitney test.
(E) Representative images of PC12 cells uptake Transferrin and 70 kD dextran for 15 min at 37°C vs at 39-40°C without preincubation. N = 3 independent experiments, n = 45 cells. Scale bar, 10 µm.
(F) Quantification of uptake of PC12 cells uptake Transferrin for 15 min at 37°C vs 39-40°C without the 3 hour-long preincubation. ns-not significant, , Mann–Whitney test.
(G) Quantification of uptake of PC12 cells uptake 70 kDa dextran for 15 min at 37°C vs at 39-40°C without the 3 hour-long preincubation. ****P < 0.0001, Mann–Whitney test.

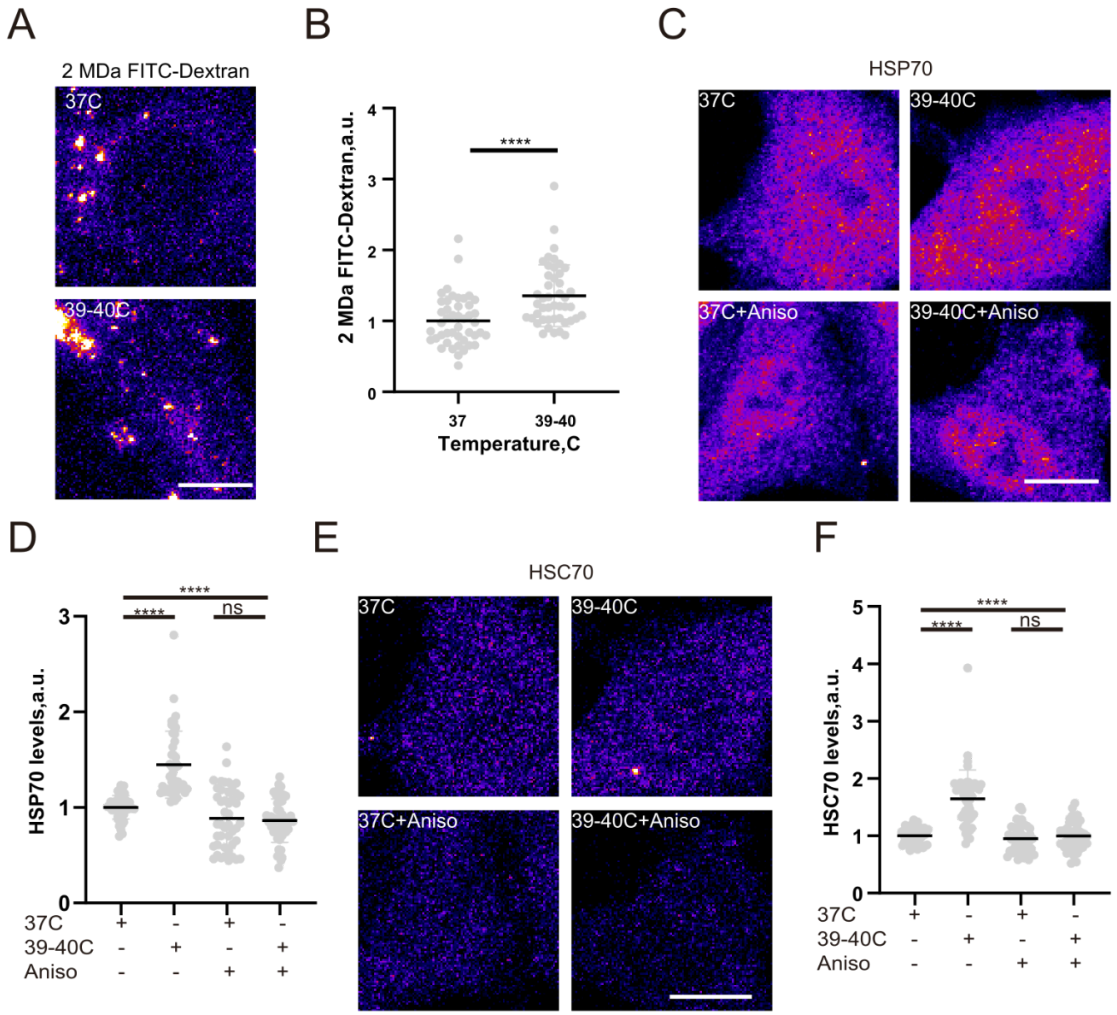

Figure S2

(A) Representative images of 2 MDa FITC-dextran internalisation in PC12 cells treated with hyperthermia for 3 hours.
(B) Quantification of 2 MDa FITC-dextran endocytosis.****P < 0.0001, Mann–Whitney test.
(C) Representative images of HSP70 in PC12 cells treated with hyperthermia for 3 hours and anisomycin.

(D) Quantification of HSP70 levels in PC12 cells treated with hyperthermia for 3 hours and anisomycin. ****P < 0.0001, ns-not significant, Kruskal–Wallis test with Dunn's multiple comparisons test.
(E) Representative images of HSC70 levels in PC12 cells treated with hyperthermia for 3 hours and anisomycin.
(F) Quantification of HSC70 levels in PC12 cells treated with hyperthermia for 3 hours and anisomycin.****P < 0.0001, ns-not significant, Kruskal–Wallis test with Dunn's multiple comparisons test.

N ≥ 3 independent experiments, n = 45 cells. Scale bar, 10 μm.

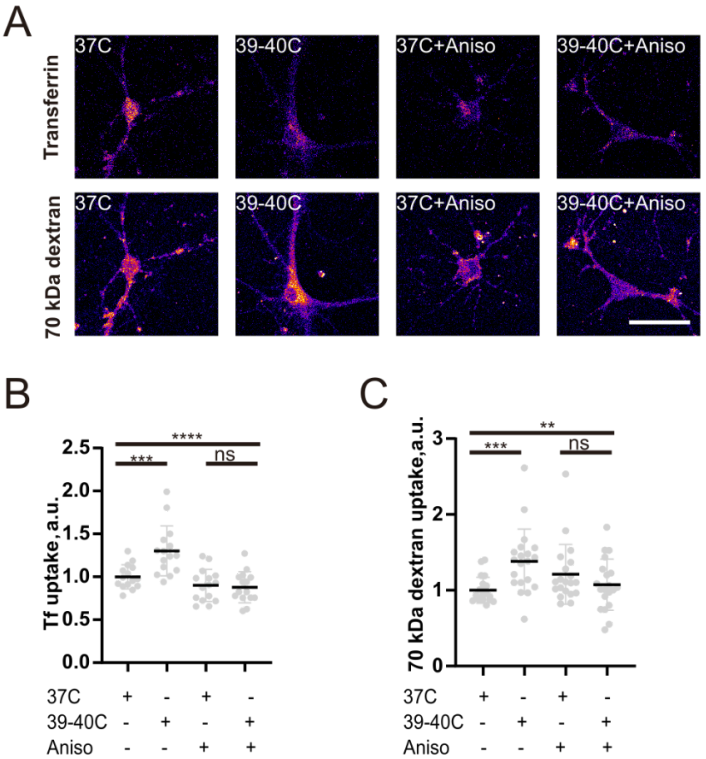

Figure S3

(A) Representative images of FITC-transferrin and 70 kDa TRITC-dextran internalisation in primary neurons treated with hyperthermia for 3 hours and anisomycin.
(B) Quantification of FITC-transferrin internalisation in primary neurons treated with hyperthermia for 3 hours with 5 anisomycin. ****P < 0.0001,***P < 0.001, ns-not significant, Kruskal–Wallis test with Dunn's multiple comparisons test.
(C) Quantification of 70 kDa TRITC-dextran internalisation in primary neurons treated with hyperthermia for 3 hours with anisomycin.***P < 0.001,**P < 0.01, ns-not significant, Kruskal–Wallis test with Dunn's multiple comparisons test.

N ≥ 3 independent experiments, n ≥ 15 cells. Scale bar, 50 μm.

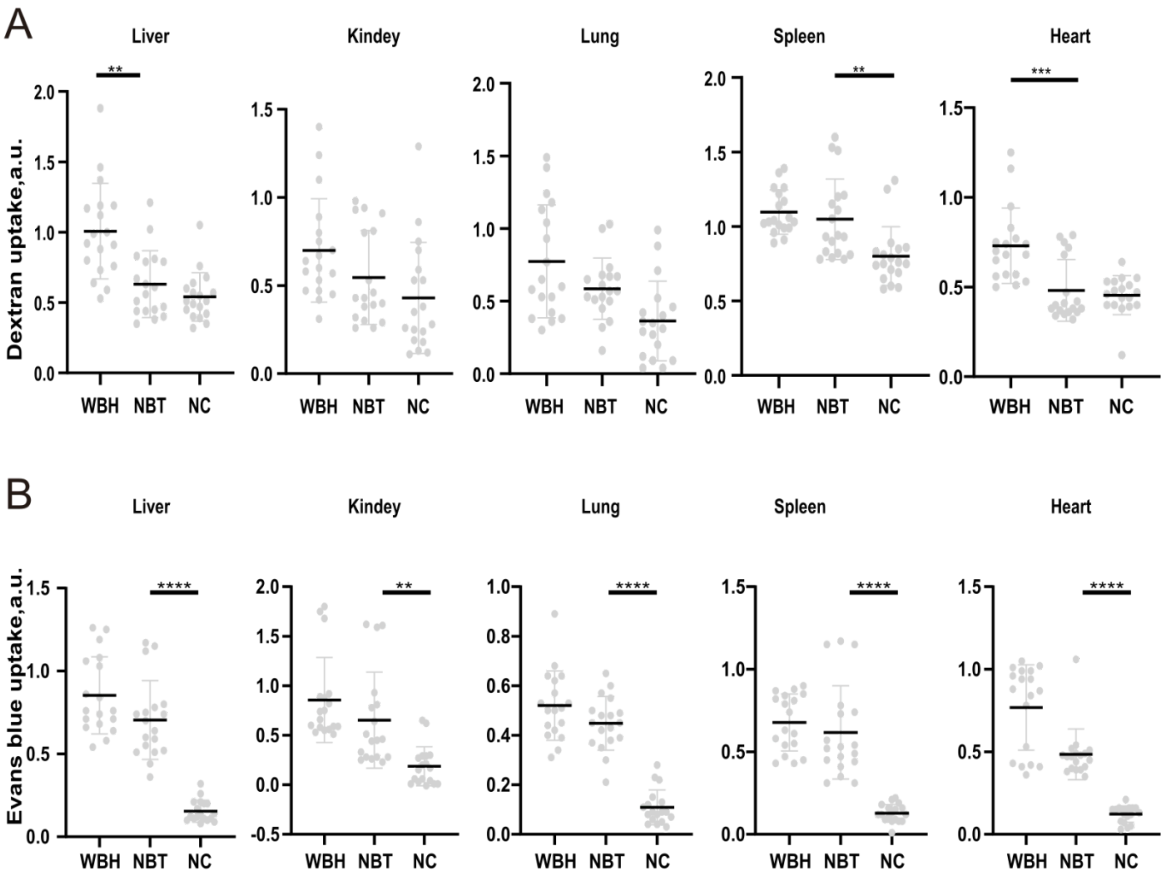

Figure S4. Data for WBH effect on dextran + Evans blue uptake from organs.

(A) Quantification of FITC signal in organs of mice injected intraperitoneally 24 hours prior to 6 hours of WBH. ***P<0.001, **P<0.01, Kruskal–Wallis test with Dunn's multiple comparisons test. 6 animals/condition.

(B) Quantification of Evans blue in organs of mice injected intraperitoneally 24h prior to 6 hours of WBH. ****P<0.0001, **P<0.01, Kruskal–Wallis test with Dunn's multiple comparisons test. 6 animals/condition.

References

1. D. Ogoina, *J. Infect. Public Health*. **4**, 108–124 (2011).
2. B. Circiumaru, G. Baldock, J. Cohen, *Intensive Care Med.* **25**, 668–673 (1999).
3. P. J. Young, M. Saxena, *Crit. Care*. **18**, 206 (2014).
4. Y. Epstein, R. Yanovich, *N. Engl. J. Med.* (2019), doi:10.1056/NEJMra1810762.
5. M. W. Dewhirst *et al.*, in *Holland-Frei Cancer Medicine. 6th edition* (BC Decker, 2003; https://www.ncbi.nlm.nih.gov/books/NBK13056/).
6. S. Balli, K. R. Shumway, S. Sharan, in *StatPearls* (StatPearls Publishing, Treasure Island (FL), 2024; http://www.ncbi.nlm.nih.gov/books/NBK562334/).
7. A. Zeiner *et al.*, *Arch. Intern. Med.* **161**, 2007–2012 (2001).
8. E. J. Walter, M. Carraretto, *Crit. Care*. **20**, 199 (2016).
9. N. Badjatia, *Crit. Care Med.* **37**, S250 (2009).
10. J. Lundgren, M.-L. Smith, G. Blennow, B. K. Siesjö, *Exp. Brain Res.* **99**, 43–55 (1994).
11. E. J. Walter, S. Hanna-Jumma, M. Carraretto, L. Forni, *Crit. Care*. **20**, 200 (2016).
12. Guidelines for evaluation of new fever in critically ill adult patients: 2008 update from

the American College of Critical Care Medicine and the Infectious Diseases Society of America - PubMed, (available at https://pubmed.ncbi.nlm.nih.gov/18379262/).
13. A. M. Vicedo-Cabrera *et al.*, *Nat. Clim. Change*. **11**, 492–500 (2021).
14. J. Ballester *et al.*, *Nat. Med.* **29**, 1857–1866 (2023).
15. S. Wrotek, E. K. LeGrand, A. Dzialuk, J. Alcock, *Evol. Med. Public Health*. **9**, 26–35 (2020).
16. Hyperthermia to Treat Cancer - NCI (2011), (available at https://www.cancer.gov/about-cancer/treatment/types/hyperthermia).
17. R. P. Patrick, T. L. Johnson, *Exp. Gerontol.* **154**, 111509 (2021).
18. E. G. P. M. de Bont *et al.*, *BMJ Open*. **5**, e007365 (2015).
19. D. R. Kaul, S. A. Flanders, J. M. Beck, S. Saint, *J. Gen. Intern. Med.* **21**, 1184–1187 (2006).
20. E. A. Kiyatkin, *Curr. Neurovasc. Res.* **1**, 77–90 (2004).
21. S. Y. Lee, S. H. Lee, K. Akuta, M. Uda, C. W. Song, *Int. J. Hyperth. Off. J. Eur. Soc. Hyperthermic Oncol. North Am. Hyperth. Group*. **16**, 73–83 (2000).
22. E. Walter, M. Carraretto, *J. Intensive Care Soc.* **16**, 306–311 (2015).
23. J. Sevigny *et al.*, *Nature*. **537**, 50–56 (2016).
24. S. Ayloo, C. Gu, *Curr. Opin. Neurobiol.* **57**, 32–38 (2019).
25. The blood–brain barrier: structure, regulation, and drug delivery | Signal Transduction and Targeted Therapy, (available at https://www.nature.com/articles/s41392-023-01481-w).
26. A. C. Anselmo, Y. Gokarn, S. Mitragotri, *Nat. Rev. Drug Discov.* **18**, 19–40 (2019).
27. O. Y *et al.*, *Int. J. Hyperth. Off. J. Eur. Soc. Hyperthermic Oncol. North Am. Hyperth. Group*. **12** (1996), doi:10.3109/02656739609022521.
28. N. McDannold, N. Vykhodtseva, F. A. Jolesz, K. Hynynen, *Magn. Reson. Med.* **51**, 913–923 (2004).
29. E. A. Kiyatkin, H. S. Sharma, *Neuroscience*. **161**, 926–939 (2009).
30. R. Yarwood, J. Hellicar, P. G. Woodman, M. Lowe, *Dis. Model. Mech.* **13**, dmm043448 (2020).
31. A. C. Yang *et al.*, *Nature*. **583**, 425–430 (2020).
32. W. D. Dietrich, R. Busto, M. Halley, I. Valdes, *J. Neuropathol. Exp. Neurol.* **49**, 486–497 (1990).
33. Z. Feng, L. Saha, C. Dritsa, Q. Wan, O. O. Glebov, *Front. Cell. Neurosci.* **16** (2022) (available at https://www.frontiersin.org/articles/10.3389/fncel.2022.1009970).
34. B. J. Galletta, J. A. Cooper, *Curr. Opin. Cell Biol.* **21**, 20–27 (2009).
35. J. J. Rennick, A. P. R. Johnston, R. G. Parton, *Nat. Nanotechnol.* **16**, 266–276 (2021).
36. K. Takahashi *et al.*, *Biochem. Biophys. Res. Commun.* **391**, 382–7 (2010).
37. J. S. Wadia, R. V. Stan, S. F. Dowdy, *Nat. Med.* **10**, 310–315 (2004).
38. S. Lindquist, *Annu. Rev. Biochem.* **55**, 1151–1191 (1986).
39. J. D. Hasday, I. S. Singh, *Cell Stress Chaperones*. **5**, 471–480 (2000).
40. Protocol for fever-range whole-body hyperthermia (WBH) in mice to study febrile effect on T-cell adhesion and migration, (available at https://star-protocols.cell.com/protocols/900).
41. W. Du *et al.*, *Mol. Psychiatry* (2024), doi:10.1038/s41380-024-02626-1.
42. M. Djaldetti, H. Bessler, *Scand. J. Clin. Lab. Invest.* (2015) (available at https://www.tandfonline.com/doi/full/10.3109/00365513.2015.1052550).
43. J. B. Smith, R. P. Knowlton, S. S. Agarwal, *J. Immunol. Baltim. Md 1950*. **121**, 691–694 (1978).
44. M. Shafaq-Zadah, E. Dransart, L. Johannes, *Curr. Opin. Cell Biol.* **65**, 112–121 (2020).
45. A. Kvalvaag *et al.*, *Proc. Natl. Acad. Sci. U. S. A.* **120**, e2211368120.
46. J. Cendrowski, A. Mamińska, M. Miaczynska, *Cytokine Growth Factor Rev.* **32**, 63–73 (2016).
47. Y. Kobayashi *et al.*, *Immunol. Lett.* **162**, 256–261 (2014).
48. D. Umar *et al.*, *Proc. Natl. Acad. Sci.* **117**, 22357–22366 (2020).
49. P. Cossart, A. Helenius, *Cold Spring Harb. Perspect. Biol.* **6**, a016972 (2014).

50. Cellular proteostasis: degradation of misfolded proteins by lysosomes | Essays in Biochemistry | Portland Press, (available at https://portlandpress.com/essaysbiochem/article/60/2/173/78290/Cellular-proteostasis-degradation-of-misfolded).
51. L. B. Persson, V. S. Ambati, O. Brandman, *Cell*. **183**, 1572-1585.e16 (2020).
52. I. El-Battrawy *et al.*, *PLoS ONE*. **11**, e0166143 (2016).
53. J. A. Lamas, L. Rueda-Ruzafa, S. Herrera-Pérez, *Int. J. Mol. Sci.* **20**, 2371 (2019).
54. V. L. Vega, W. Charles, A. De Maio, *Cell Stress Chaperones*. **15**, 517–527 (2010).
55. E. Eisenberg, L. E. Greene, *Traffic*. **8**, 640–646 (2007).
56. N. Mounier, A.-P. Arrigo, *Cell Stress Chaperones*. **7**, 167–176 (2002).
57. A. De Maio, L. Hightower, *Cell Stress Chaperones*. **26**, 769–783 (2021).
58. S. Welker *et al.*, *Mol. Cell*. **39**, 507–520 (2010).
59. S. Lu *et al.*, *Nat. Cell Biol.* **24**, 1378–1393 (2022).
60. A. L. Darling *et al.*, *Protein Sci. Publ. Protein Soc.* **30**, 1350–1359 (2021).
61. J. Gu *et al.*, *Proc. Natl. Acad. Sci.* **117**, 31123–31133 (2020).
62. A. C. Martins, F. Albericio, B. G. de la Torre, *Biomedicines*. **11** (2023), doi:10.3390/biomedicines11051434.
63. S. Kaech, G. Banker, *Nat. Protoc.* **1**, 2406–15 (2006).